Journal of Hazardous Materials 436 (2022) 129084

Contents lists available at ScienceDirect

Journal of Hazardous Materials

journal homepage: www.elsevier.com/locate/jhazmat

Research Paper

Fate of face masks after being discarded into seawater: Aging and microbial colonization

Jie Ma[a], Fengyuan Chen[a], Huo Xu[a], Jingli Liu[a], Ciara Chun Chen[a], Zhen Zhang[a], Hao Jiang[b], Yanping Li[a], Ke Pan[a,*]

[a] Shenzhen Key Laboratory of Marine Microbiome Engineering, Institute for Advanced Study, Shenzhen University, Shenzhen 518060 Guangdong, China
[b] Key Laboratory of Aquatic Botany and Watershed Ecology, Wuhan Botanical Garden, Chinese Academy of Sciences, Wuhan 430074 Hubei, China

HIGHLIGHTS

- Facemasks were exposed in natural seawater, and their aging and effects on the microbial community were evaluated.
- Floating masks undergone significant aging and developed specific fouling organisms on the surfaces within one month.
- The facemasks discarded in coastal waters eventually sink to the seabed within one month.
- This study lays the groundwork for mask-pollution management and future research.

GRAPHICAL ABSTRACT

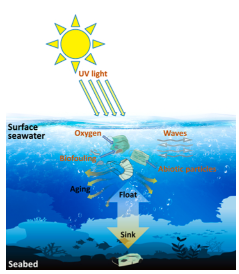

ARTICLE INFO

Editor: Teresa A.P. Rocha-Santos

Keywords:
Masks
Plastic pollution
Aging
Marine environment
Microbials

ABSTRACT

Billions of discarded masks have entered the oceans since the outbreak of the COVID-19 pandemic. Current reports mostly discuss the potential of masks as plastic pollution, but there has been no study on the fate of this emerging plastic waste in the marine environment. Therefore, we exposed masks in natural seawater and evaluated their aging and effects on the microbial community using a combination of physicochemical and biological techniques. After 30-day exposure in natural seawater, the masks suffered from significant aging. Microbial colonizers such as Rhodobacteraceae Flavobacteriaceae, Vibrionaceae and fouling organisms like calcareous tubeworms *Hydroides elegans* were massively present on the masks. The roughness and modulus of the mask fiber increased 3 and 5 times, respectively, and the molecular weight decreased 7%. The growth of biofouling organisms caused the masks negatively buoyant after 14–30 days. Our study sheds some light on the fate of discarded masks in a coastal area and provides fundamental data to manage this important plastic waste during COVID-19 pandemic.

1. Introduction

Billions of face masks have been used daily since the outbreak of the COVID-19 pandemic (Carias et al., 2015; Adyel, 2020). The cheap price of surgical masks facilitates their use, but people discard them casually. It is reported that about 1.56 billion facemasks entered the oceans in

* Corresponding author.
E-mail address: panke@szu.edu.cn (K. Pan).

https://doi.org/10.1016/j.jhazmat.2022.129084
Received 28 March 2022; Received in revised form 30 April 2022; Accepted 3 May 2022
Available online 5 May 2022

2020 (Bondaroff and Cooke, 2020). In the following year, another research estimated that 0.15–0.39 million tons of mask debris (equivalent to 3.3–8.7 billion surgical masks) could end up in global oceans within a year (Chowdhury et al., 2021). Therefore, the fate of discarded masks in environment is an increasing concern (Aragaw, 2020; Fadare and Okoffo, 2020).

Discarded masks can easily exacerbate the scourge of plastic pollution (Hernandez et al., 2017; Parashar and Hait, 2021). Most masks are made of three or more layers of polypropylene (PP) in fiber structures, although cotton fibers, polystyrene, polycarbonate, polyethylene, or polyester are also used. The structure of a typical surgical mask includes outer and inner spun-bond layers in the front and back with fiber diameters of 20–30 μm, as well as a middle melt-blown layer with fiber diameter around 2 μm (Hutten, 2007). Studies have detected microplastics (MPs) that are released from plastic products such as cosmetics and water bottles (Karami et al., 2017; Mason et al., 2018; Koelmans et al., 2019). Recently, researches on plastic teabags and infant feeding bottles have found that they can release millions to billions of MPs when they are immersed in or contain hot liquid, which causes thermal aging (Hernandez et al., 2019; Li et al., 2020).

Several studies have demonstrated that masks can release nanoplastics, MPs, additives, and heavy metals into environments (Liu et al., 2021; Morgana et al., 2021; Sullivan et al., 2021; Wang et al., 2021). These substances could generate adverse effects on both terrestrial and marine organisms (Kwak and An, 2021; Sun et al., 2021). However, most of the studies were conducted in laboratory and the fate of discarded masks in natural environments remain unexplored. Particularly, the physiochemical changes of the nano-sized mask fibers and succession of microorganisms on the fibers has not been examined. But this information could be important for understanding the effects of discarded masks on the environment.

In these circumstances, we exposed masks in natural seawater and monitored them weekly. Using scanning electron microscopy (SEM) and atomic force microscopy (AFM), the aging of the masks was evaluated according to the nano topographic and mechanical changes on their surfaces, and the chemical changes of the masks were analyzed by X-ray photoelectron spectroscopy (XPS) and Fourier-transform infrared spectroscopy (FTIR). The microbial communities on the masks were investigated based on MiSeq high-throughput sequencing. We also tried to figure out when the masks sink from the surface seawater to the seabed. This is the first time series study on the nano scale surface aging and colonization on masks in natural marine environment and contributes to the understanding of this emerging plastic pollution from the COVID-19 pandemic.

2. Materials and methods

2.1. Mask collection and aging in natural seawater

Facemask samples were purchased from a local online retailer in June 2020. These surgical-grade and N95 masks were made for adults and had three layers: two spun-bond inner and outer layers and one melt-blown middle layer. The instructions on the package indicated that the masks were made of non-woven PP, except for the inner layer of N95 masks, which was made of cotton). To observe the aging of facemasks in a marine environment, batches of 10 facemasks (3 surgical masks for each brand, and 4 N95 masks) were put into nylon mesh bags (10 bags in total). The bags were submerged under the surface of coastal waters in Dapeng Bay on the eastern side of Hong Kong in July 2020. The weather in the following month was steady at the sampling site (average temperature: 29 °C, cloudy or sunny, breeze). Every week, 10 randomly selected facemasks were retrieved from the sea and transported to the laboratory in a cooler box.

2.2. Density determination of the masks

To measure the changes in density, mask samples were freeze-dried, and the dry mass (m) was measured first. Then they were totally immersed into 200 mL (v_1) 75% alcohol in a 250 mL graduated cylinder, where the alcohol solution can easily infiltrate the samples and avoid the air bubbles. After 2 h infiltration, the volume (v_2) was determined. The sample density (ρ) was calculated by the formula:

$\rho = m/(v_2 - v_1)$.

Six replications were set for each treatment.

2.3. Removal of biofouling from aged facemask fibers

To evaluate the aging process of facemask fibers, the biofouling on the masks was carefully removed according to an established procedure (Wang et al., 2017; Scheurer and Bigalke, 2018). Each facemask (with all three layers) was cut into 1-cm × 1-cm sheets at the midsection, and each sheet was rinsed three times using seawater that had been passed through a 0.22-μm filter. The sheet sample was then immersed in Milli-Q water for 1 h and transferred into a clean glass vial containing 15 mL of hydrogen peroxide solution (H_2O_2, w/w 30%).

The vial was tightly sealed and heated in an oven at 55 °C for 7 days. Then, the sample was digested for another 7 days with an additional 5 mL of H_2O_2 (Allen et al., 2019). After the digestion, the facemask sheet was rinsed with Milli-Q water and dried with pure ethanol. The sheet was transferred into a clean glass vial containing $ZnCl_2$ solution with a density of 1.6 g mL^{-1} and agitated on an orbit shaker (60 rpm) for 7 days at room temperature. Finally, the suspended sheet was again rinsed with Milli-Q water, dried with pure ethanol, and subjected to the series of tests described below. As a control, new facemask sheets were treated using the same cleaning procedure.

2.4. Surface characterization of facemask fibers by SEM and AFM

The surfaces of cleaned facemask samples were observed by FE-SEM (Tescan, MIRA3, Oxford, Czech Republic). Briefly, the samples were sputter-coated with a 3-nm layer of Pt. The accelerating voltage was set at 5 kV, and all images were captured within 30 s to minimize electron-beam damage to the sample surface.

The nanostructures and nanomechanical properties (roughness, Young's modulus, and adhesion) of facemask fibers were analyzed by an AFM (Dimension icon, Bruker, Santa Barbara, CA, USA). AFM was conducted in peak force quantitative nanomechanical mapping mode using a TAP150A probe (Bruker, tip radius: 5 −15 nm, frequency 150 kHz, spring constant of 5 N/m). The probe was calibrated according to the manufacturer's instructions prior to measurements, and the scan rate was set at 1 Hz. Maps of roughness, adhesion, and Young's modulus were acquired from an area of 2 × 2 μm^2.

A nanoindentation experiment was then performed to evaluate the fragility of the facemask fibers. A diamond-coated probe (DDESP-V2) was used, and the spring constant of the probe's cantilever was 97 N m^{-1}. The ramp rate and size were 1 Hz and 2 μm, respectively. The force that pressed against the surface of the masks was 15 μN. This preloaded force was strong enough to generate a marked indent on the fiber surface. The hardness of the fiber was calculated according to Oliver and Pharr (1992) using the following formula:

$$H = \frac{F_{max}}{A}$$

where F_{max} is the peak indentation load when generating an indent on a diatom frustule, and A is the projected area of the hardness impression. All AFM measurements were performed in air at room temperature and approximately 50% relative humidity. Six randomly selected surfaces were measured for each treatment (n = 6). NanoScope Analysis software

(Version 1.4, Bruker) was used to analyze the acquired AFM data.

2.5. Measurement of surface chemical composition of the facemask fiber

High-temperature gel permeation chromatography (GPC, PL-GPC 220, Agilent, California, USA) with three PL gel MIXED-BLS columns (300 × 7.5 mm, 10 μm) was used to measure the z-average (M_z), weight-average (M_w), and number-average (M_n) molecular weights and dispersities (M_w/M_n) of the facemask fibers. The measurements were conducted at 150 °C using trichlorobenzene as the mobile phase at a flow rate of 1 mL min^{-1}.

The surface chemical composition of the facemask fibers was characterized by X-ray photoelectron spectroscopy (XPS) and FTIR. The binding states of selected elements of carbon (C 1 s), oxygen (O 1 s), nitrogen (N 1 s), silicon (Si 2p), sulfur (S 2p), phosphorus (P 2p), and calcium (Ca 2p) of the facemask fibers were examined by XPS. Briefly, a 1-cm^2 facemask sheet was placed on an aluminum platform, and a non-monochromatic aluminum K_α-source (1486.6 eV) was used as the excitation energy source. The characterization was done at a power of 300 W. The X-ray spot on the sample was about 1 mm^2, and the photoelectrons were collected at a depth of 100 Å with a take-off angle of 53°.

The XPS spectra were calibrated to the standard C (1 s) peak at 284.6 eV caused by unaffected aliphatic carbon adsorbates. Data processing was performed with AVANTAGE software (Thermo Fisher Scientific, East Grinstead, UK). The peaks were decomposed by performing the first trial without constraints and fitting with a known number of similar full width at half maximum (FWHM) components. Peaks with distances less than 0.5 eV between each other were identified as the same component. The backgrounds were fitted using Shirley backgrounds, and the measurement was repeated three times to ensure reproducibility. FTIR was conducted using an instrument with a single-bounce diamond (PerkinElmer) in an attenuated total reflection (ATR) sampling accessory. The spectra were collected between 4000 and 650 cm^{-1} at a resolution of 4 cm^{-1}.

2.6. Analysis of microbial communities on masks

High-throughput sequencing of 16 S rRNA genes was employed to investigate the temporal changes of microbial communities on the facemask fibers that occur when floating in the surface seawater. Briefly, a freshly collected facemask was cut into 1-cm^2 sheets at the midsection and used for total DNA extraction with a DNeasy Power Biofilm Kit (Qiagen) according to the manufacturer's recommended protocols. The hypervariable V4 region of the 16 S rRNA genes was amplified with primer pairs 515 F and 806 R (Walters et al., 2016). PCR reactions were performed in triplicate.

After gel purification, the PCR products were pooled in equimolar concentrations and subjected to sequencing on the Illumina MiSeq PE300 platform according to the standard protocols (Majorbio Bio-Pharm Technology Co. Ltd., Shanghai, China). Sequences were quality filtered and clustered into operational taxonomic units (OTUs) with a cutoff of 97% similarity using UPARSE (version 7.1) (Edgar, 2013). The taxonomy of each representative OTU sequence was analyzed by RDP Classifier (version 2.2) against the Silva database v138 using a threshold of 70% similarity (Wang et al., 2007). We also examined co-occurrence patterns using network analysis.

2.7. Functional prediction of microbial communities using 16S rRNA gene sequences

To investigate the microbial community's functional capabilities, PICRUSt predictions (Douglas et al., 2020) were performed using the OTU table (the top-100 most abundant OTUs, representing 47% of the total microbial community; Table S2). The table contains Green gene identifiers (Desantis et al., 2006) that match the marker gene with the OTU abundances across samples. Briefly, gene families present in organisms were first predicted based on the genes observed in the reference genomes of their sequenced evolutionary relatives and their functional categorized KEGG ortholog (KO) abundances (Markowitz et al., 2012). OTU abundances were then normalized based on the abundance of each organism and its predicted 16 S rRNA gene copy number. After multiplying the normalized OTU abundance by each KO abundance in reference genomes, these KO abundances were summed together for each sample.

2.8. Statistical analysis

Differences in rates or concentrations between treatments were statistically compared using a one-way or two-way ANOVA in RStudio. Data were tested for normality using the Shapiro−Wilks test as appropriate. A student's *t*-test was used to determine whether treatments were significantly different. A co-occurrence network of microbial communities at the OTU level was constructed to identify the underlying associations among the microbial taxa. All of the graphical and statistical analyses were performed using a series of R packages (phyloseq, ggplot2, and vegan).

3. Results

3.1. Macroscopic changes of masks after exposure in natural seawater

The most visible change on the mask surfaces after exposure in seawater was the formation of biofilm and biofouling (Figs. 1 and S1–2). Biofilm began to form within the first 7 days and increased during the

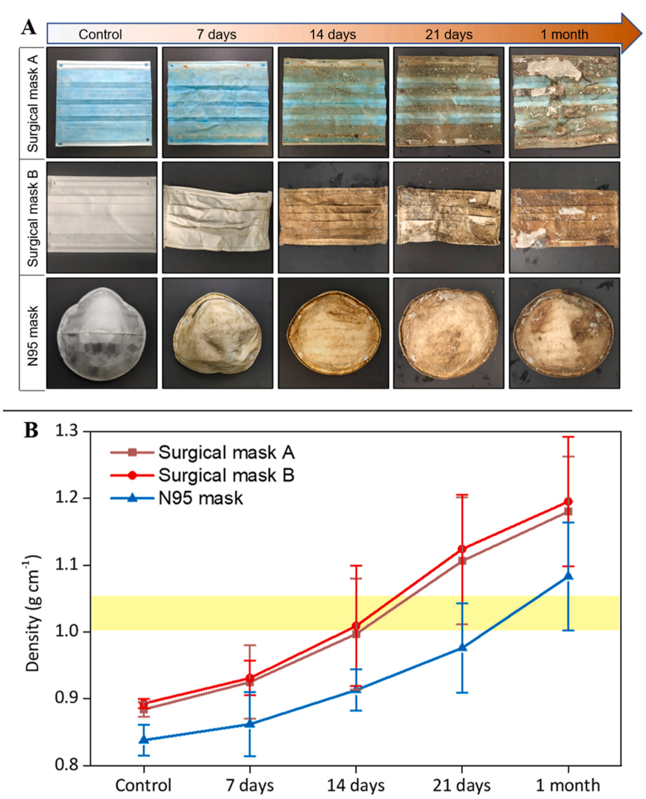

Fig. 1. The changes of different types of masks before and after exposure in coastal seawater. (A) Macroscopic observation showing the plastic yellowing and matter adhering to the surface of the samples after 7, 14, and 21 days and 1 month of exposure. (B) The changes of buoyancy of the samples after 7, 14, and 21 days and 1 month of exposure. Yellow shading shows neutral buoyancy of 1.0–1.05 in seawater. Data are shown as the mean ± SD (n = 6). Asterisks denote a significant difference ($p < 0.05$).

experiment. By 14 days, calcified structures had gradually appeared on the surfaces of masks (Fig. 1). After 1 month, other typical biofouling organisms such as larvae and spores were observed (Fig. 1 and S1). SEM images further showed the attachment of various fouling organisms such as calcified tube worms, diatoms, and resting cysts of dinoflagellates (Fig. S1).

The dry weight of a typical surgical mask was significantly increased from 3.2 ± 0.11 g to 4.3 ± 0.38 g after 14 days and further increased to 5.8 ± 0.60 g after 1 month (Fig. S3A). More critically, the densities of surgical and N95 masks were 0.89 ± 0.09 and 0.84 ± 0.02 g cm^{-3} dry weight, respectively, which were lower than that of seawater (1.05 g cm^{-3}). Their densities all surpassed 1.05 g cm^{-3} after 1 month, suggesting that facemasks in coastal waters will eventually sink to the seabed. But surgical masks tended to sink more rapidly than N95 masks (Fig. 1B), and the individual layers of the surgical masks sank even more quickly (Fig. S3B). In addition, little difference was found between the outer and inner surfaces of masks in the process of biofouling (Fig. 1 and S4). Details of the fouling microbials' taxa on exposed masks are described in the following experiment of high-throughput sequencing of 16 S rRNA genes.

3.2. Micro and nano surface morphology and mechanical properties

The SEM images show that the fibers of new masks' three layers exhibited relatively smooth surface textures (Fig. S5). For the outer and inner layers that were directly exposed to UV light, flakes appeared on their surfaces after only 7 days in seawater. The defective area then expanded over time. In the middle layer, which was shielded between the outer and inner layers, cracks were found after 21 days, and further fiber breaks occurred within 1 month (Fig. S5).

AFM was employed to investigate the surface morphology and mechanical properties. At the nano scale, the three layers of the masks exhibited similar defects. The representative morphology images showed the presence of nodules after 14 days, and nano pits appeared at 21 days, which became bigger holes after 1 month (Fig. 2A). The surface roughness was analyzed on the morphology images, which showed significant increases in roughness from 1.2 ± 0.3 nm for new masks to 2.0 ± 0.4, 3.6 ± 0.4, and 3.5 ± 1.1 nm for masks after 14 days, 21 days, and 1 month in seawater, respectively (Fig. 2B).

The surface's Young's modulus, which reflects the mechanical strength, became more heterogeneous over time (Fig. 2A). The average surface modulus significantly increased from 2.6 ± 0.2 GPa for new masks to 5.4 ± 1.1, 9.2 ± 1.5, and 11.3 ± 3.4 GPa for masks after 14 days, 21 days, and 1 month, respectively (Fig. 2 C). In contrast, the adhesion slightly decreased from 66.7 ± 6.3 nN for new masks to 60.1 ± 4.8 nN for masks after 14 days and significantly decreased to 51.8 ± 6.4 and 47.3 ± 2.4 nN after 21 days and 1 month, respectively (Fig. 2D). Indentation results indicated that the surface hardness significantly increased from 0.4 ± 0.2 GPa for new masks to 1.1 ± 0.1 and 1.7 ± 0.2 GPa for masks after 21 days and 1 month, respectively (Fig. 3).

3.3. Chemical changes on mask surfaces

The molecular weight of masks decreased over time after immersion in seawater (Table 1). For the outer and inner spun-bond layers, the original molecular weight (M_w) was much higher at 176,936 g mol^{-1} than that of the melt-blown layer at 67,802 g mol^{-1}. The spun-bond layer also had higher M_w/M_n (MWD) ratios of 2.24–2.41 than the melt-blown layer at 1.92–2.09, but the MWD ratios varied among the samples with different seawater-exposure times.

The new masks were almost pure carbon (C) structural materials with only 1.22% atomic percentage of oxygen. After exposure, changing proportions of oxygen (O), nitrogen (N), phosphorus (P), sulfur (S),

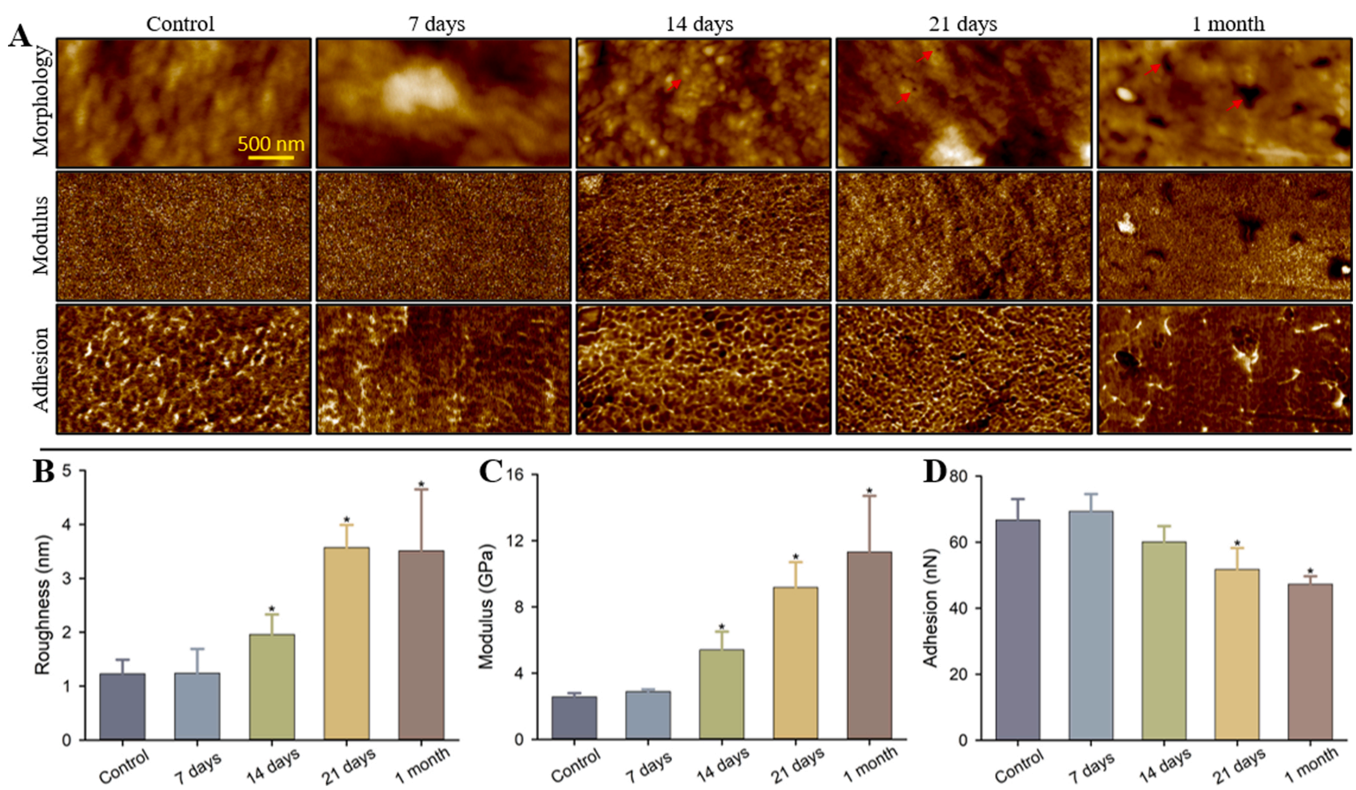

Fig. 2. Atomic force microscope (AFM) images showing the nano-scale changes of mask surfaces before and after 7, 14, and 21 days and 1 month in coastal seawater. (A) AFM morphology images and corresponding modulus and adhesion mapping of the mask surfaces. The red arrows in (A) show aging-generated nodules and pits. (B–D) The quantitative nano mechanical properties of roughness (B), modulus (C), and adhesion (D) of the exposed masks. Data are shown as the mean ± SD (n = 6). Asterisks denote a significant difference ($p < 0.05$).

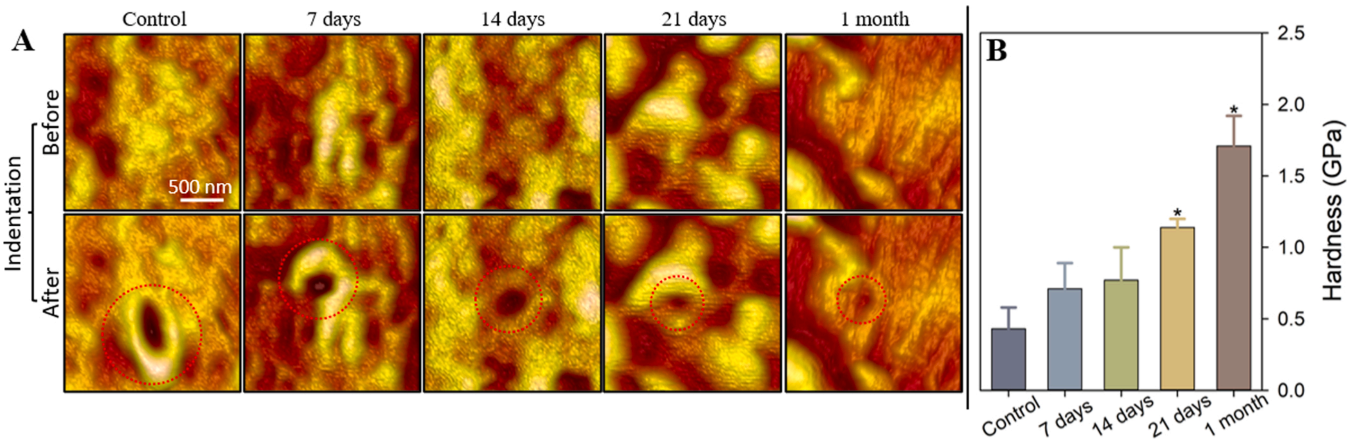

Fig. 3. The hardness of mask surfaces was measured by AFM nano-indentation before and after 7, 14, and 21 days and 1 month in coastal seawater. (A) Nano-surfaces of masks and the corresponding surfaces after indentation. Red circles show the indent holes formed by an AFM tip. (B) Calculated hardness from (A). Data are shown as the mean ± SD (n = 6). Asterisks denote a significant difference ($p < 0.05$).

Table 1
Molecular characteristics of spun-bond and melt-blown layers of masks before and after 7, 14, and 21 days and 1 month sampling in seawater (mean ± SD, n = 3).

Sampling time	Masks layers	M_z (g mol^{-1})[a]	M_w (g mol^{-1})[b]	M_n (g mol^{-1})[c]	M_w/M_n (MWD)[d]
0	Spun-bond (S)	346,207 ± 2283	176,936 ± 1817	78,981 ± 596	2.24 ± 0.03
	Melt-blown (M)	109,713 ± 740	67,802 ± 1046	35,304 ± 541	1.92 ± 0.02
7 days	S	325,529 ± 2517	175,398 ± 1386	76,887 ± 1141	2.28 ± 0.04
	M	106,741 ± 1066	63,781 ± 635	30,447 ± 623	2.09 ± 0.08
14 days	S	314,823 ± 1712	170,696 ± 2610	70,738 ± 1679	2.41 ± 0.03
	M	93,646 ± 1258	57,618 ± 827	30,218 ± 548	1.91 ± 0.02
21 days	S	311,371 ± 1343	170,444 ± 1165	73,520 ± 1852	2.32 ± 0.04
	M	89,096 ± 1162	54,058 ± 943	25,963 ± 794	2.08 ± 0.10
1 month	S	301,049 ± 3310	167,583 ± 1495	73,773 ± 1967	2.27 ± 0.07
	M	87,413 ± 1282	53,668 ± 745	27,310 ± 935	1.97 ± 0.05

[a] Size average (M_z): Polymer's toughness; [b] Weight average (M_w): Polymer's melt viscosity, brittleness and chemical resistance; [c] Number average (M_n): Polymer's flexural strength.; [d] M_w/M_n: Homogeneity.

silicon (Si), and calcium (Ca) were detected on the surfaces of masks over time (Table 2, Fig. S6A). Specifically, the analysis of elemental chemical states showed an increasing component near 287.8 eV, which was attributed to double bonds of C with O. Furthermore, the N proportion increased over time, which was decomposed into two components near 400.0 eV and 402 eV, which were attributed to amine functions and protonated amine, respectively. The smaller proportions of phosphate groups and sulfide of peptide ($S_{2p3/2}$ at 163.8 eV) were also increased over time. Although the proportion of Si remained low (0.2%), there was an increase in its contribution at 103.1 eV, which was attributed to silica. Ca had relative atomic proportions of 0.2% and 0.5% in 7 and 14-day samples and increased to 1.6% and 0.9% in the 21-day and 1-month samples, respectively (Table 2).

Chemical changes on the masks' surfaces were also characterized by ATR-FTIR (Fig. S6B). The IR spectra of new masks and masks exposed within 14 days were congruent with a pure PP reference, in which the typical vibration bands of CH, CH_2, and CH_3 stretching (2839–2953 cm^{-1}) and bending (1376–1457 cm^{-1}) were clearly visible (Käppler et al., 2018). After 21 days in seawater, overlapping spectral bands were observed in the fingerprint region of 900–1800 cm^{-1}, which could be due to a number of undetermined types of environmental organic components (Käppler et al., 2016). At the same time, the typical PP spectral pattern disappeared due to the thick biofilm that covered the mask surfaces. In addition, peaks at 712 and 869 cm^{-1} were characterized as $CaCO_3$, which could be responsible for the increasing density of the masks (Battegazzore et al., 2020).

3.4. *Microbial community on the masks*

Based on the exposure days, the alpha diversity of bacteria was measured using three indices: the Shannon, ACE, and Chao indices. The results show that after 21 days in seawater, the masks exhibited the highest alpha diversity of bacteria (the largest number of detected OTUs; Table S1). The communities' beta diversity was compared through a principal coordinate analysis (PCoA) (Fig. S7).

Using Bray Curtis dissimilarity, the first two principal components explained 41.89% of the community variance. Permutational multivariate analysis of variance (PERMANOVA) was used to calculate significant differences between these community dissimilarities ($p = 0.001$). The seawater community and the community on the masks after 7 days in sweater were in the bottom-right quadrant, while the communities on the masks after 14 and 21 days were in the left. The community on the masks after 1 month was distinctly different from the others and was in the top-right quadrant (Fig. S7). This indicated that when the masks were kept in seawater, the communities on them exhibited significant changes over time.

At the class level, Gammaproteobacteria (relative abundance: 20%−36%), Bacteroidia (13%−21%), and Alphaproteobacteria (15%−20%) dominated the bacteria communities in all samples (Fig. S8). The relative abundances of Clostridia were 5% and 12% on 7 and 14-day samples, respectively. Relative abundances of 4%, 2%, and 9% of Campylobacteria were found in samples at 7 days, 14 days, and 1 month, respectively (Fig. S8).

At the family level, the relative abundance of families at > 1% is illustrated in Fig. 4. In all samples, higher relative abundance of the families Rhodobacteraceae and Flavobacteriaceae was found. Vibrionaceae was also found in all samples, but its highest relative abundance in the masks was exhibited after 1 month.

The 7-day sample had one unique family, Oleiphilaceae, while the 14-day sample had four exclusive families: Clostridiaceae, Holosporaceae, Shewanellaceae, and Fusobacteriaceae. The 21-day sample had six exclusive families: Coleofasciculaceae, Tenderiaceae, Woeseiaceae,

Table 2
X-ray photoelectron spectroscopy (XPS) spectral parameters of the mask surfaces (the outer layer) after seawater exposure over time.

Element	Core-level	Assignment[a]	Control			7 days			14 days			21 days			1 month		
			AP[b] (%)	BE[c] (eV)	CD[d] (%)	AP (%)	BE (eV)	CD (%)	AP (%)	BE (eV)	CD (%)	AP (%)	BE (eV)	CD (%)	AP (%)	BE (eV)	CD (%)
C	1 s	Aromatic **C**-H,[1]	98.8	284.1	2.1	74.3	284.1	6.3	71.8	284.1	5.8	66.5	284.1	11.8	61.6	284.1	15.8
		Aliphatic **C**-H,[1]		284.9	94.9		284.9	81.0		284.9	60.2		284.9	58.3		284.9	42.4
		C-(O, N),[1,2]		285.9	1.7		285.9	5.3		286.3	22.1		286.3	17.7		286.2	28.3
		C=O,[1,]		287.8	1.3		287.7	7.4		287.7	7.9		287.9	9.0		287.9	11.2
		O-**C**=O,[1]								288.9	3.9		289.0	3.2		288.9	2.3
O	1 s	**O**-C,[1,3]	1.2			18.7	531.8	50.2	20.5	531.8	58.5	23.3	531.7	60.3	24.1	531.6	66.2
		O=C,[1,3]		532.8	100		533.0	49.8		533.0	41.5		533.0	39.7		532.8	33.8
N	1 s	**N**-C,[2,4]				5.6	400.0	88.3	6.0	400.1	78.3	7.1	399.9	96.1	11.8	399.8	68.4
		O=C-**N**H_2,[2,4]					402.1	11.7		402.0	21.7		401.8	3.9		401.7	31.6
P	2p	Phosphate groups,[2]				0.5	133.6		0.6	133.5		0.9	133.3		0.9	133.4	
S	2p	**S**-C,[2]				0.5	163.9	14.8	0.4	163.9	37.6	0.4	163.8	40.1	0.5	163.9	52.2
		SO_4^{2-},[2]					168.8	85.2		168.9	62.4		168.8	59.9		169.0	47.8
Si	2p	**Si**-OH,[2]				0.2	102.1	92.9	0.2	102.3	44.7	0.2	102.3	45.9	0.2	102.2	40.8
		SiO_2,[2]					103.0	7.1		103.1	55.3		103.1	54.1		103.0	59.2
Ca	2p					0.2	347.3		0.5	347.3		1.6	347.3		0.9	347.3	

a: references for the assignment of binding energy are shown in the supporting information. b: AP: atomic percentage; c: BE: binding energy; d: CD: component distribution; that is, the proportion of each component peak. Corresponding references in assignment column: 1. Liu et al., 2019; 2. Tesson et al., 2009; 3. Chen et al. (2021); 4. Mutel et al. (2000) (these references can be found in supplementary information).

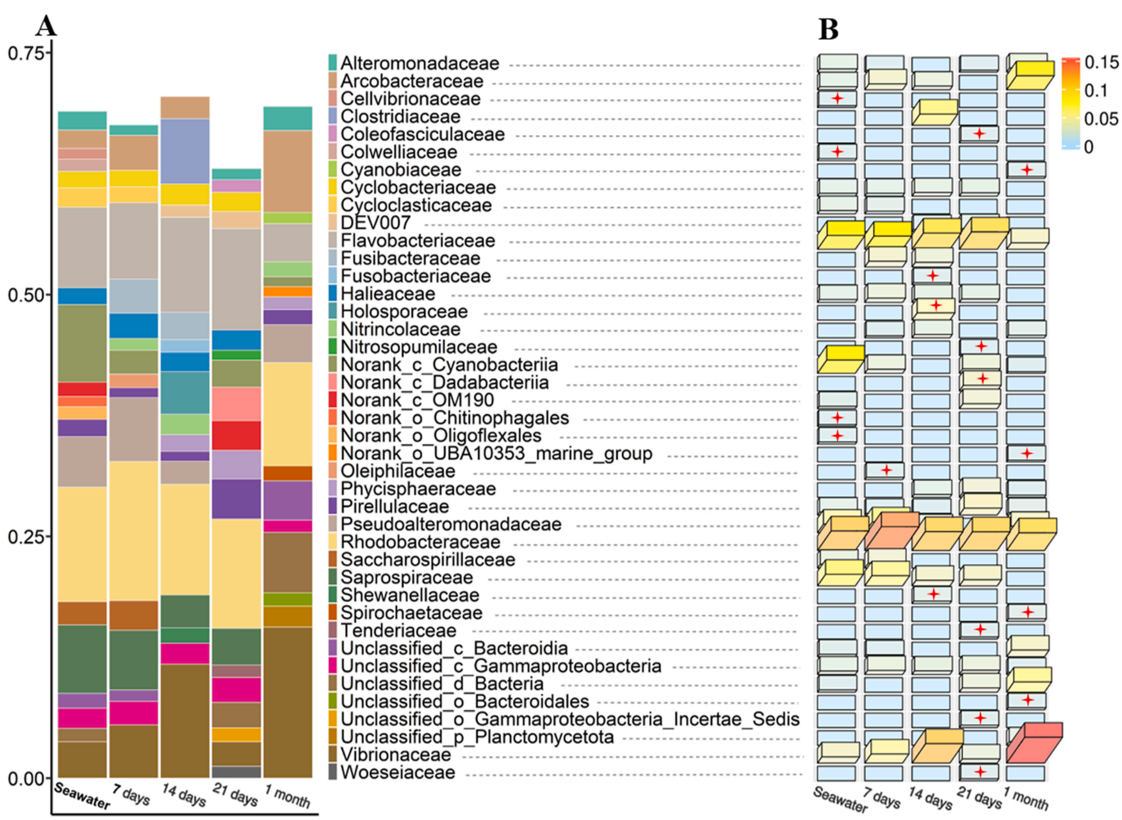

Fig. 4. Composition of prokaryotic community inhabiting masks after 7, 14, and 21 days and 1 month in coastal seawater. (A) Stacked bar plot showing the relative abundance of families with average abundance > 1% (n = 3) for each sample-collection date (7, 14, and 21 days and 1 month). (B) Corresponding heat map showing the difference in relative abundance between treatments. Asterisks in (B) represent the unique OTUs for each treatment.

Nitrosopumilaceae, a no-rank family belonging to the class Dadabacteriia, and an unclassified family belonging to order Gammaproteobacteria incertae sedis. Finally, the 1-month sample had five exclusive families: Spirochaetaceae, Cyanobiaceae, two unclassified families belonging to the phylum Planctomycetota and order Bacteroidales, and a no-rank family belonging to the order UBA10353 marine group. More details about the microbials of the plastisphere on the exposed masks can be seen in the supporting information (Figs. S9, S10, and Table S2).

Using the sequenced reference genomes (top-100 most abundant OTUs, Table S2), PICRUSt predictions were analyzed to obtain biological insights. The abundance of KEGG pathways is shown in Fig. 5, which illustrates that the genes involved in metabolisms were most abundant, followed by those involved in cellular, environmental information, and genetic information processes. Lasty, pathways related to biodegradation processes in the plastisphere also showed up, such as xenobiotic

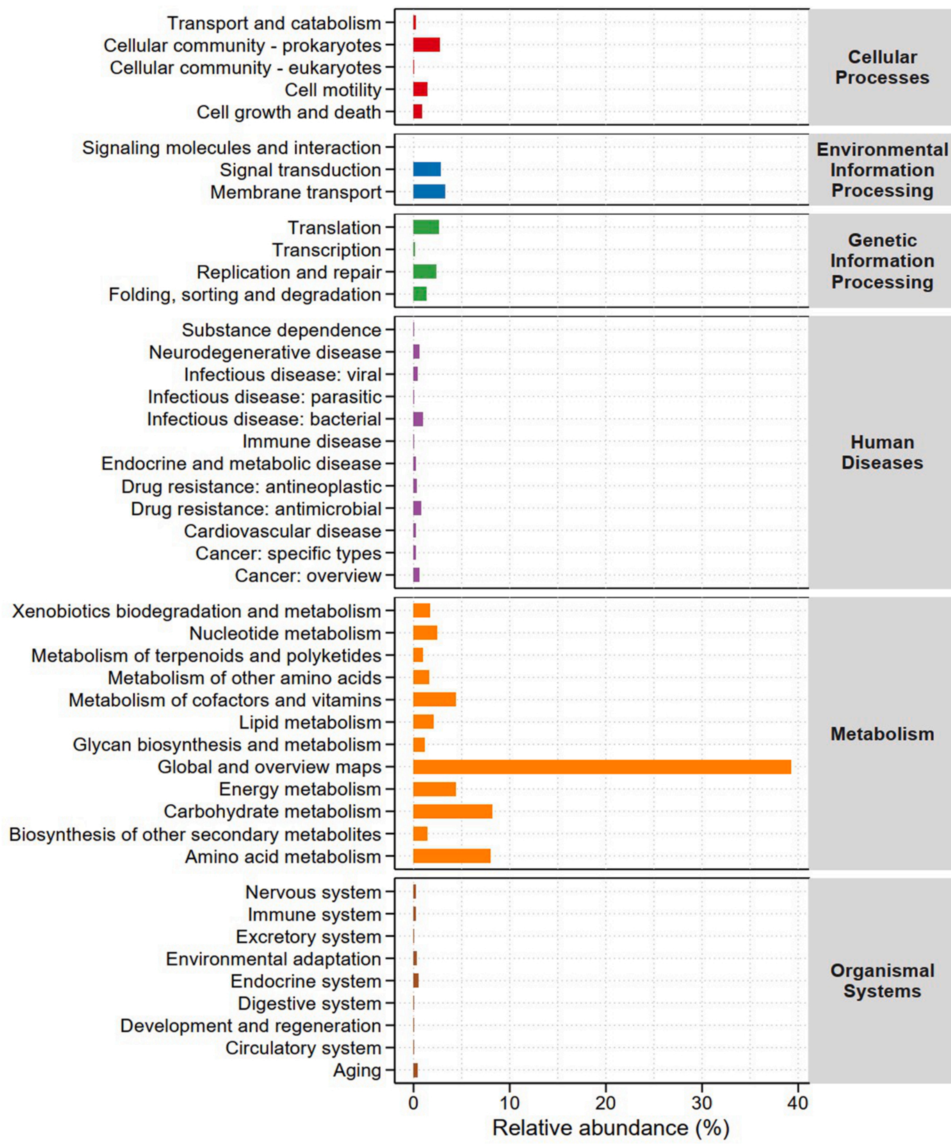

Fig. 5. Functional categories of microbes on mask-surface samples kept in seawater. The data were generated based on the 16 S genomes of top-100 most abundant OTUs of the samples. The relative abundance refers to the percent of total abundance assigned to each category.

biodegradation and metabolism processes.

4. Discussion

Studies have shown that after entering the marine environment, plastic wastes may have different fates depending on their characteristics (Fadare and Okoffo, 2020). High-density plastics such as polyethylene terephthalate (PET), polyvinyl chloride (PVC), and polystyrene (PS) are likely to sink and reach the bottom marine sediments, while less dense polymers like PP (with a density of about 0.9 g cm^{-3}) will float in seawater (De-la-Torre and Aragaw 2021). It has been demonstrated that biofouling causes plastics to lose buoyancy, thus leading them to sink in seawater (Kowalski et al., 2016; Chen et al., 2019). Investigations have already found that PP from discarded masks accumulates as waste in both the surface seawater and seabed, indicating a change of their buoyancy in seawater (Aragaw, 2020).

Our macroscopic observation showed significant amounts of fouling on the masks' surfaces (Fig. 1 and S1), and the chemical and microbial investigation indicated the formation of surface-attached biofilms (Fig. 4, S2, and S6). Microbials may have a neutral effect on buoyancy of the colonized masks, but the aggregation of calcified organisms and inorganic particles could have a negative effect on buoyancy and result in their sinking (Figs. 1B and S1–3). For example, a high amount of *Hydroides elegans* was found among the fouling organisms (Fig. S1). A previous study found that this species has a generation time of about 3 weeks in response to natural biofilms formed by marine bacterial species (Nedved and Hadfield, 2008). This is the same time scale as that in which the buoyancy of masks became negative, indicating that its calcareous tubes have a profound influence on the fate of masks in the marine environment.

Masks floating in surface seawater are exposed to strong UV radiation and oxidizing conditions, which have been noted as fundamental factors that initiate the aging of plastics (Singh and Sharma, 2008; Gewert et al., 2015). We found that continuous aging of the PP fibers of masks began in the first 7 days in seawater (Fig. 2 and S5, Table 1). Interestingly, the aging seemed faster than that of other plastic samples from previous studies. For example, Song et al. (2017) found cracks on PE pellet surfaces after 6 months of UV exposure. Cai et al. (2018) exposed PP pellets to UV irradiation in laboratory seawater, and flakes and cracks appeared on samples after 1 month of exposure. O'Brine and Thompson (2010) showed that biodegradable plastic bags began to aging within 28 days in natural seawater. Indeed, as polymer with stable tertiary carbons, PP is thought to age slow in the marine environment (Bond et al., 2018), where the aging rate for PP is estimated at 4.6–7.5 μm $year^{-1}$ (Chamas et al., 2020). Large plastics could still be an integrity piece after a long-time. However, the mask fibers with diameter around 3 μm were broken within 30 days.

Several factors could contribute to the aging of masks in the marine environment. As most plastics first aging on the polymer surface, the aging proceeds are faster for microplastics than meso- and macroplastics due to the higher surface-to-volume ratio (Gewert et al., 2015). Compared with other plastic products, masks have a net structure with higher net density and smaller fiber size. A typical surgical mask can provide a large surface area of 1.4×10^4 cm^2, which is 14 times larger than that of a 500-mL plastic bottle (see SI for the estimation of the surface area of a mask). These features could contribute to their release of substantial MPs, especially under the initial UV-oxidation aging processes before they sinking down to the seabed (Ma et al., 2021; Sun et al., 2021; Wang et al., 2021). Furthermore, mechanical action by waves in natural seawater can accelerate the carbon chain scission of the polymers, especially for masks that are made of soft microfibers. Generally, the observed biofouling could also play important roles in biodegradation of masks. Organisms with hard tissues can physically penetrate the mask fibers. On the other hand, excretions such as exoenzymes and lipophilic pigments from microorganisms may corrode the polymer (Shah et al., 2008; Jacquin et al., 2019). More bioinformatic analysis will be discussed later.

At the nano scale, AFM investigation revealed the masks' aging as the surface morphology and physical properties significantly changed (Figs. 2 and 3). Combining our results with previous researches (Singh and sharma, 2008; Gewert et al., 2015; Wang et al., 2021), Fig. 6 illustrates the putative aging process of mask fibers in seawater. Initially, free radicals could be formed when UV radiation breaks C-H bonds on the mask fibers. Next, the neighboring carbon chains with free radicals could crosslink with each other, especially in the aquatic environment, where there may be less oxygen than that in the air. This crosslinking may contribute to the increase of the modulus (Fig. 2B, Fig. 3), which could lead to embrittlement of the mask fibers (Najafi et al., 2006; Signoret et al., 2020). With oxygen, the polymer forms peroxyl radicals, ultimately resulting in chain scission (Gewert et al., 2015), which could explain the observed nodules and pits in AFM (Fig. 2). Therefore, crosslinking, chain scission, branching, and formation of oxygen-containing functional groups develop on the mask surfaces, resulting in higher surface roughness due to the generated nano-granular oxidation, pits, and flakes (Zbyszewski et al., 2014; Cai et al., 2018). The rougher surface supplies an enlarged surface area for UV radiation and oxygen, which further accelerates the aging (Gatenholm et al., 1997). In accordance with these results, the molecular weight of the masks decreased over time in seawater (Table 1), which reflected that the masks becoming brittle along with the carbon chain actions (Summer and Rabinovitch, 1999). However, more research efforts are needed to clarify these aging processes.

Physical changes on mask surfaces occurred in parallel with elemental and chemical variations. As discussed above, UV-oxidative aging of masks can form oxygen-containing functional groups (Singh and Sharma, 2008). The gradually increasing abundance of element and functional groups reflects both the marine organisms and abiotic particles adhering on the surfaces of masks (Figs. S1, S2, S6 and Table 2). The intrusion of biofilm on mask surfaces could also offer various functional groups (Lang et al., 2020; Chen et al., 2021). The generated groups such as carbonyl can enhance the hydrophilicity of mask surfaces and might increase their availability for biodegradation (Karian, 2003). Moreover, the increasing N proportion provides a favorable C/N ratio for biodegradation (Sauret et al., 2016). These chemical changes indicate that floating masks in seawater can be covered by biofilms of microbials and fouling organisms, and although the biofilms might shield the masks from UV radiation, further biodegradation might take place (Shah et al., 2008; Gewert et al., 2015).

The differences between the microbial communities of surrounding seawater and samples notably increased over time (Fig. S7), indicating that specific microbials prefer to colonize mask surfaces, for example, the highest abundant species in Vibrionaceae family. Moreover, the microbial community succession on the masks can be explained in part due to the competition of microbials or grazing by ciliates, vertebrates,

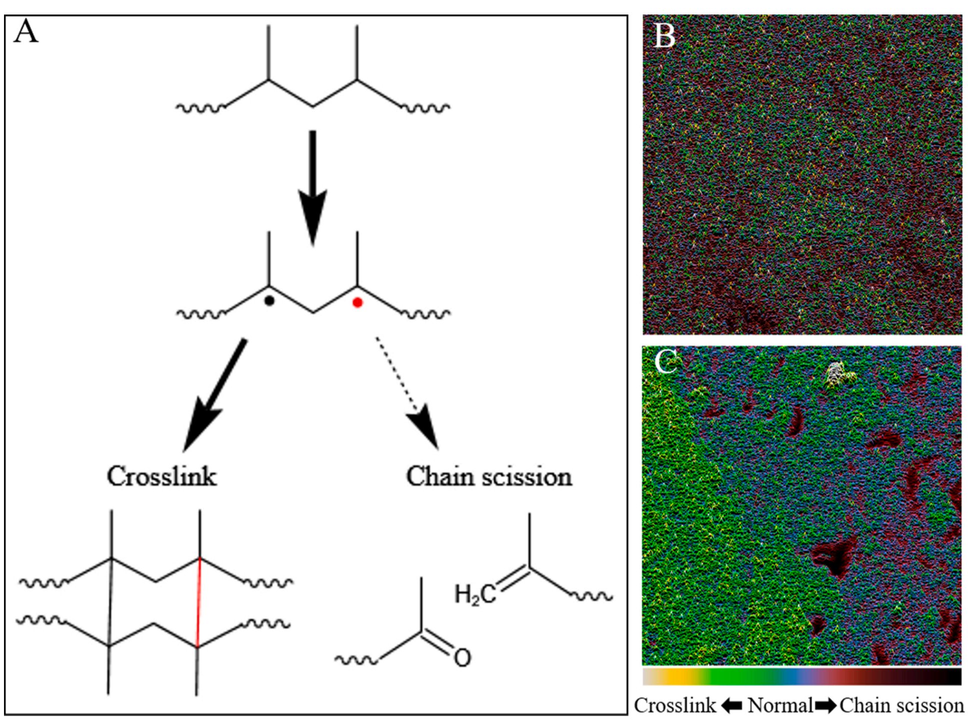

Fig. 6. Illustration of the putative aging pathways of polypropylene (PP) masks. (A) Chemical structure of PP and its summary of aging. (B) Representative image derived from AFM modulus mapping showing the typical initial fiber surface of a mask. (C) Corresponding surface image after 1 month in seawater, where crosslinking (green and yellow), chain scission (deep red and black) occurred.

and other grazers, which play a role in transforming the community composition (Schmidt et al., 2014; Amaral-Zettler et al., 2015).

Another possible explanation is that UV-oxidative aging generated oligomers or monomers on the surfaces of masks (Fig. 2 and S5), and there could be increased numbers of microbials that use enzymes to further fragmentize polymers or directly use monomers as a carbon source (Dussud and Ghiglione, 2014). It can be hypothesized that the biofilms may retard the formation of these oligomers in the microenvironment of mask surfaces and provide enough dissolved organic carbon to support prokaryotic metabolism and establish biodegradation pathways (Arrieta et al., 2015; Bryant et al., 2016). Therefore, variable communities on masks appeared to develop characteristic taxa over time, and evolutionary adaption to mask aging is expected (Yoshida et al., 2016; Oberbeckmann and Labrenz, 2020).

Based on our 16 S rRNA sequence data, a putative network of mask-related microbials is given in Fig. S11. Taxa in our network were similar to those in previous studies on plastispheres, which covered bacterial strains living on plastics that have the capability to biodegrade plastic or are associated with biodegradation (Zettler et al., 2013; Krueger et al., 2015; Bryant et al., 2016; Dussud et al., 2018). Among these taxa, the families Rhodobacteraceae, Flavobacteriaceae, and Vibrionaceae were found to be the core taxa on the mask surfaces (Fig. 4, Table S2). Members of these families can alternate between planktonic and attached lifestyles and are thus capable of rapidly colonizing artificial surfaces (Dang et al., 2008; Elifantz et al., 2013).

The mechanisms of biodegradation involved in the enzymatic fragmentation of polymers. However, this could be a very long process that lasts decades or even hundreds of years (Barnes et al., 2009; Andrady, 2015). In the short term, microbial-secreted enzymes have a limited effect on changing the mechanical, physical, and chemical properties (Andrady, 2017). Hence, the colonizing microbials reported here are more likely to be consumers with the potential to utilize the monomers produced by UV-oxidative aging (Fig. 5) instead of playing a leading role in masks' aging.

Another important concern is the colonization of pathogenic microbials on the masks. We found a dominance of the family Vibrionaceae, which constituted 16% of the community on the mask surfaces after 1 month (Fig. 4). Suspected pathogenic microbials in the families Arcobacteraceae and Shewanellaceae were also present on the mask surfaces (Fig. 4).

The *Vibrio* strains could be animal or human pathogens and cannot be found in such a high concentration in a natural community (Thompson and Polz, 2006). However, the genus *Vibrio* blooms on PP debris in the marine environment (Zettler et al., 2013). This is not only due to their fast growth rate, but also their ability to dominate surface phytoplankton and zooplankton (Polz et al., 2006; Preheim et al., 2011). Senderovich et al. (2010) found human pathogenic *Vibrio* strains in fishes, and news and reports have shown that both fishes and birds can ingest mask wastes or their debris. Combined with the fact that PP masks persist longer than natural substrates (e.g., feathers, wood, and macroalgae) and may travel long distances before sinking, they could serve as a vector of infectious diseases through the marine food chain (Barnes and Jerez, 2002).

5. Conclusions

Discarded masks in surface seawater were exposed to strong UV radiation and dissolved oxygen, and these two factors greatly accelerated their aging process. The photo-oxidation and physical disintegration increased the surface roughness and decreased the molecular weight of masks fibers. Then, the aged surface and generated fragments became more susceptible to biodegradation.

The increasing density of masks due to biofouling results in their sinking within 1 month in seawater, which is a crucial event that delivers the masks to different layers of the ocean and dramatically increases the polluted area. In addition, the biofilm formed by microbials on masks made them a niche plastisphere environment that could dramatically influence the microbial community and aging process of masks. With nutrients and marine organisms on their surfaces, masks could be eaten by mistake by marine animals such as fishes, birds, or even mammals like whales, which has already been reported in news and surveys. Although the change of destiny of masks in the marine environment may vary in different areas due to different UV-radiation levels, temperatures, and biotic community structures, our study has shown a glance at the fate of discarded masks in a coastal area and provided fundamental data for management strategies.

Environmental implication

Since the outbreak of COVID-19, billions of used facemasks have been released into oceans. To date, no study has evaluated the fate of masks in the marine environment. In this study, we exposed masks in natural seawater, and evaluated their aging and effects on the microbial community. The results demonstrated that the masks in seawater aged significantly after 30-days exposure in seawater. Fouling organisms developed on mask surfaces and resulted in the negative buoyance of the masks. Masks could act as carriers of potential pathogenic bacteria in marine environment. This study lays the groundwork for mask-pollution management and future research.

CRediT authorship contribution statement

Ke Pan and Jie Ma designed the research. Jie Ma, Huo Xu, Ciara Chun Chen, Zhen Zhang, and Yanping Li performed the experiments. Jie Ma, Fengyuan Chen, Jingli Liu, and Hao Jiang analyzed data. Jie Ma and Ke Pan wrote the manuscript.

Declaration of Competing Interest

The authors declare that they have no known competing financial interests or personal relationships that could have appeared to influence the work reported in this paper.

Acknowledgements

This work was supported by the Shenzhen Science and Technology Innovation Commission of China (JCYJ20180507182227257 and KQTD20180412181334790), National Natural Science Foundation of China (41976140, 42076148, 42006141), the Guangxi Key Research and Development Program of China (GUIKE AB20297018), Guangdong Basic and Applied Basic Research Foundation (2019A1515011630).

Appendix A. Supporting information

Supplementary data associated with this article can be found in the online version at doi:10.1016/j.jhazmat.2022.129084.

References

Adyel, T.M., 2020. Accumulation of plastic waste during COVID-19. Science 369 (6509), 1314–1315.
Allen, S., Allen, D., Phoenix, V.R., Le Roux, G., Jiménez, P.D., Simonneau, A., Binet, S., Galop, D., 2019. Atmospheric transport and deposition of microplastics in a remote mountain catchment. Nat. Geosci. 12 (5), 339–344.
Amaral-Zettler, L.A., Zettler, E.R., Slikas, B., Boyd, G.D., Melvin, D.W., Morrall, C.E., Proskurowski, G., Mincer, T.J., 2015. The biogeography of the Plastisphere: implications for policy. Front. Ecol. Environ. 13 (10), 541–546.
Andrady, A.L., 2015. Persistence of plastic litter in the oceans. Marine Anthropogenic Litter. Springer, pp. 57–72.
Andrady, A.L., 2017. The plastic in microplastics: a review. Mar. Pollut. Bull. 119 (1), 12–22.
Aragaw, T.A., 2020. Surgical face masks as a potential source for microplastic pollution in the COVID-19 scenario. Mar. Pollut. Bull. 159, 111517.
Arrieta, J.M., Mayol, E., Hansman, R.L., Herndl, G.J., Dittmar, T., Duarte, C.M., 2015. Dilution limits dissolved organic carbon utilization in the deep ocean. Science 348 (6232), 331–333.

Barnes, D.K.A., Jerez, D., 2002. Biodiversity: Invasions by marine life on plastic debris. Nature 416 (6883), 808–809.

Barnes, D.K.A., Galgani, F., Thompson, R.C., Barlaz, M., 2009. Accumulation and fragmentation of plastic debris in global environments. Philos. Trans. R. Soc. Lond. B 364 (1526), 1985–1998.

Battegazzore, D., Cravero, F., Frache, A., 2020. Is it possible to mechanical recycle the materials of the disposable filtering masks? Polymers 12 (11), 2726.

Bond, T., Ferrandiz-Mas, V., Felipe-Sotelo, M., Van Sebille, E., 2018. The occurrence and degradation of aquatic plastic litter based on polymer physicochemical properties: A review. Crit. Rev. Env. Sci. Tec 48 (7−9), 685–722.

Bondaroff, T.P., Cooke, S., 2020. Masks on the beach: the impact of COVID-19 on marine plastic pollution. OceansAsia.

Bryant, J.A., Clemente, T.M., Viviani, D.A., Fong, A.A., Thomas, K.A., Kemp, P., Karl, D. M., White, A.E., DeLong, E.F., 2016. Diversity and activity of communities inhabiting plastic debris in the North Pacific Gyre. MSystems 1 (3), e00024–16.

Cai, L., Wang, J., Peng, J., Wu, Z., Tan, X., 2018. Observation of the degradation of three types of plastic pellets exposed to UV irradiation in three different environments. Sci. Total Environ. 628, 740–747.

Carias, C., Rainisch, G., Shankar, M., Adhikari, B.B., Swerdlow, D.L., Bower, W.A., Pillai, S.K., Meltzer, M.I., Koonin, L.M., 2015. Potential demand for respirators and surgical masks during a hypothetical influenza pandemic in the United States. Clin. Infect. Dis. 60 (suppl_1), S42–S51.

Chamas, A., Moon, H., Zheng, J., Qiu, Y., Tabassum, T., Jang, J.H., Abu-Omar, M., Scott, S.L., Suh, S., 2020. Degradation rates of plastics in the environment. ACS Sustain. Chem. Eng. 8 (9), 3494–3511.

Chen, X., Xiong, X., Jiang, X., Shi, H., Wu, C., 2019. Sinking of floating plastic debris caused by biofilm development in a freshwater lake. Chemosphere 222, 856–864.

Chen, Y., Li, J., Wang, F., Yang, H., Liu, L., 2021. Adsorption of tetracyclines onto polyethylene microplastics: A combined study of experiment and molecular dynamics simulation. Chemosphere 265, 129133.

Chowdhury, H., Chowdhury, T., Sait, S.M., 2021. Estimating marine plastic pollution from COVID-19 face masks in coastal regions. Mar. Pollut. Bull. 168, 112419.

Dang, H., Li, T., Chen, M., Huang, G., 2008. Cross-ocean distribution of *Rhodobacterales* bacteria as primary surface colonizers in temperate coastal marine waters. Appl. Environ. Microbiol. 74 (1), 52–60.

De-la-Torre, G.E., Aragaw, T.A., 2021. What we need to know about PPE associated with the COVID-19 pandemic in the marine environment. Mar. Pollut. Bull. 163, 111879.

DeSantis, T.Z., Hugenholtz, P., Larsen, N., Rojas, M., Brodie, E.L., Keller, K., Huber, T., Dalevi, D., Hu, P., Andersen, G.L., 2006. Greengenes, a chimera-checked 16S rRNA gene database and workbench compatible with ARB. Appl. Environ. Microbiol. 72 (7), 5069–5072.

Douglas, G.M., Maffei, V.J., Zaneveld, J.R., Yurgel, S.N., Brown, J.R., Taylor, C.M., Huttenhower, C., Langille, M.G., 2020. PICRUSt2 for prediction of metagenome functions. Nat. Biotechnol. 38 (6), 685–688.

Dussud, C., Ghiglione, J.F., 2014. Bacterial degradation of synthetic plastics. CIESM Workshop Monogr. Vol. 46, pp. 49−54.

Edgar, R.C., 2013. UPARSE: highly accurate OTU sequences from microbial amplicon reads. Nat. Methods 10 (10), 996–998.

Elifantz, H., Horn, G., Ayon, M., Cohen, Y., Minz, D., 2013. *Rhodobacteraceae* are the key members of the microbial community of the initial biofilm formed in eastern Mediterranean coastal seawater. FEMS Microbiol. Ecol. 85 (2), 348–357.

Fadare, O.O., Okoffo, E.D., 2020. Covid-19 face masks: a potential source of microplastic fibers in the environment. Sci. Total Environ. 737, 140279.

Gatenholm, P., Ashida, T., Hoffman, A.S., 1997. Hybrid biomaterials prepared by ozone-induced polymerization. I. Ozonation of microporous polypropylene. J. Polym. Sci. Pol. Chem. 35 (8), 1461–1467.

Gewert, B., Plassmann, M.M., MacLeod, M., 2015. Pathways for degradation of plastic polymers floating in the marine environment. Environ. Sci. Processes Impacts 17 (9), 1513–1521.

Hernandez, L.M., Nariman, Y., Nathalie, T., 2017. Are there nanoplastics in your personal care products? Environ. Sci. Technol. Lett. 4 (7), 280–285.

Hernandez, L.M., Xu, E.G., Larsson, H.C., Tahara, R., Maisuria, V.B., Tufenkji, N., 2019. Plastic teabags release billions of microparticles and nanoparticles into tea. Environ. Sci. Technol. 53 (21), 12300–12310.

Hutten, I.M., 2007. Handbook of Nonwoven Filter Media. Elsevier, pp. 195–244.

Jacquin, J., Cheng, J., Odobel, C., Pandin, C., Conan, P., Pujo-Pay, M., Barbe, V., Meistertzheim, A.-L., Ghiglione, J.-F., 2019. Microbial ecotoxicology of marine plastic debris: a review on colonization and biodegradation by the "plastisphere". Front. Microbiol. 10, 865.

Käppler, A., Fischer, D., Oberbeckmann, S., Schernewski, G., Labrenz, M., Eichhorn, K.J., Voit, B., 2016. Analysis of environmental microplastics by vibrational microspectroscopy: FTIR, Raman or both? Anal. Bioanal. Chem. 408 (29), 8377–8391.

Käppler, A., Fischer, M., Scholz-Böttcher, B.M., Oberbeckmann, S., Labrenz, M., Fischer, D., Eichhorn, K.-J., Voit, B., 2018. Comparison of μ-ATR-FTIR spectroscopy and py-GCMS as identification tools for microplastic particles and fibers isolated from river sediments. Anal. Bioanal. Chem. 410 (21), 5313–5327.

Karami, A., Golieskardi, A., Keong Choo, C., Larat, V., Galloway, T.S., Salamatinia, B., 2017. The presence of microplastics in commercial salts from different countries. Sci. Rep. 7 (1), 1–11.

Karian, H., 2003. Handbook of polypropylene and polypropylene composites, revised and expanded. CRC press.

Koelmans, A.A., Nor, N.H.M., Hermsen, E., Kooi, M., Mintenig, S.M., De France, J., 2019. Microplastics in freshwaters and drinking water: critical review and assessment of data quality. Water Res 155, 410–422.

Kowalski, N., Reichardt, A.M., Waniek, J.J., 2016. Sinking rates of microplastics and potential implications of their alteration by physical, biological, and chemical factors. Mar. Pollut. Bull. 109 (1), 310–319.

Krueger, M.C., Harms, H., Schlosser, D., 2015. Prospects for microbiological solutions to environmental pollution with plastics. Appl. Microbiol. Biotechnol. 99 (21), 8857–8874.

Kwak, J.I., An, Y.J., 2021. Post COVID-19 pandemic: Biofragmentation and soil ecotoxicological effects of microplastics derived from face masks. J. Hazard. Mater. 416, 126169.

Lang, M., Yu, X., Liu, J., Xia, T., Wang, T., Jia, H., Guo, X., 2020. Fenton aging significantly affects the heavy metal adsorption capacity of polystyrene microplastics. Sci. Total Environ. 722, 137762.

Li, D., Shi, Y., Yang, L., Xiao, L., Kehoe, D.K., Gun'ko, Y.K., Boland, J.J., Wang, J.J., 2020. Microplastic release from the degradation of polypropylene feeding bottles during infant formula preparation. Nat. Food 1 (11), 746–754.

Liu, R., Mabury, S.A., 2021. Single-use face masks as a potential source of synthetic antioxidants to the environment. Environ. Sci. Technol. Lett. 8 (8), 651–655.

Ma, J., Chen, F., Xu, H., Jiang, H., Liu, J., Li, P., Chen, C.C., Pan, K., 2021. Face masks as a source of nanoplastics and microplastics in the environment: quantification, characterization, and potential for bioaccumulation. Environ. Pollut., 117748

Markowitz, V.M., Chen, I.M.A., Palaniappan, K., Chu, K., Szeto, E., Grechkin, Y., Ratner, A., Jacob, B., Huang, J., Williams, P., Huntemann, M., Anderson, I., Mavromatic, K., Ivanova, N.N., Kyrpides, N.C., 2012. IMG: the integrated microbial genomes database and comparative analysis system. Nucleic Acids Res 40 (D1), D115–D122.

Mason, S.A., Welch, V.G., Neratko, J., 2018. Synthetic polymer contamination in bottled water. Front. Chem. 6, 407.

Morgana, S., Casentini, B., Amalfitano, S., 2021. Uncovering the release of micro/nanoplastics from disposable face masks at times of COVID-19. J. Hazard. Mater. 419, 126507.

Mutel, B., Grimblot, J., Dessaux, O., Goudmand, P., 2000. XPS investigations of nitrogen-plasma-treated polypropylene in a reactor coupled to the spectrometer. Surf. Interface Anal. 30, 401–406.

Najafi, S.K., Hamidinia, E., Tajvidi, M., 2006. Mechanical properties of composites from sawdust and recycled plastics. J. Appl. Polym. Sci. 100 (5), 3641–3645.

Nedved, B.T., Hadfield, M.G., 2008. *Hydroides elegans* (Annelida: Polychaeta): A Model for Biofouling Research. Springer Series on Biofilms. Springer, Berlin, Heidelberg, pp. 1–15.

O'Brine, T., Thompson, R.C., 2010. Degradation of plastic carrier bags in the marine environment. Mar. Pollut. Bull. 60 (12), 2279–2283.

Oberbeckmann, S., Labrenz, M., 2020. Marine microbial assemblages on microplastics: diversity, adaptation, and role in degradation. Ann. Rev. Mar. Sci. 12, 209–232.

Oliver, W.C., Pharr, G., 1992. An improved technique for determining hardness and elastic modulus using load and displacement sensing indentation. J. Mater. Res. 7, 1564.

Parashar, N., Hait, S., 2021. Plastics in the time of COVID-19 pandemic: protector or polluter? Sci. Total Environ. 759, 144274.

Polz, M.F., Hunt, D.E., Preheim, S.P., Weinreich, D.M., 2006. Patterns and mechanisms of genetic and phenotypic differentiation in marine microbes. Philos. Trans. R. Soc. B 361 (1475), 2009–2021.

Preheim, S.P., Boucher, Y., Wildschutte, H., David, L.A., Veneziano, D., Alm, E.J., Polz, M.F., 2011. Metapopulation structure of *Vibrionaceae* among coastal marine invertebrates. Environ. Microbiol 13 (1), 265–275.

Sauret, C., Tedetti, M., Guigue, C., Dumas, C., Lami, R., Pujo-Pay, M., Conan, P., Goutx, M., Ghiglione, J.F., 2016. Influence of PAHs among other coastal environmental variables on total and PAH-degrading bacterial communities. Environ. Sci. Pollut. Res. 23 (5), 4242–4256.

Scheurer, M., Bigalke, M., 2018. Microplastics in Swiss floodplain soils. Environ. Sci. Technol. 52 (6), 3591–3598.

Schmidt, V.T., Reveillaud, J., Zettler, E., Mincer, T.J., Murphy, L., Amaral-Zettler, L.A., 2014. Oligotyping reveals community level habitat selection within the genus Vibrio. Front. Microbiol. 5, 563.

Senderovich, Y., Izhaki, I., Halpern, M., 2010. Fish as reservoirs and vectors of *Vibrio* cholerae. PloS One 5, e8607.

Shah, A.A., Hasan, F., Hameed, A., Ahmed, S., 2008. Biological degradation of plastics: a comprehensive review. Biotechnol. Adv. 26 (3), 246–265.

Signoret, C., Edo, M., Lafon, D., Caro-Bretelle, A.S., Lopez-Cuesta, J.M., Ienny, P., Perrin, D., 2020. Degradation of styrenic plastics during recycling: Impact of reprocessing photodegraded material on aspect and mechanical properties. J. Polym. Environ. 28 (8), 2055–2077.

Singh, B., Sharma, N., 2008. Mechanistic implications of plastic degradation. Polym. Degrad. Stabil. 93 (3), 561–584.

Song, Y.K., Hong, S.H., Jang, M., Han, G.M., Jung, S.W., Shim, W.J., 2017. Combined effects of UV exposure duration and mechanical abrasion on microplastic fragmentation by polymer type. Environ. Sci. Technol. 51 (8), 4368–4376.

Sullivan, G.L., Delgado-Gallardo, J., Watson, T.M., Sarp, S., 2021. An investigation into the leaching of micro and nano particles and chemical pollutants from disposable face masks-linked to the COVID-19 pandemic. Water Res 196, 117033.

Summers, J.W., Rabinovitch, E.B., 1999. Weathering of Plastics. Elsevier, pp. 61–68.

Sun, J., Yang, S., Zhou, G.J., Zhang, K., Lu, Y., Jin, Q., Lam, P.K.S., Leung, K.M.Y., He, Y., 2021. Release of microplastics from discarded surgical masks and their adverse impacts on the marine copepod *Tigriopus japonicus*. Environ. Sci. Technol. Lett. 8 (12), 1065–1070.

Thompson, J.R., Polz, M.F., 2006. Dynamics of *Vibrio* Populations and Their Role in Environmental Nutrient Cycling. The Biology of Vibrios. ASM Press, Washington, DC, pp. 190–203.

Walters, W., Hyde, E.R., Berg-Lyons, D., Ackermann, G., Humphrey, G., Parada, A., Gilbert, J.A., Jansson, J.K., Caporaso, J.G., Fuhrman, J.A., Apprill, A., Knight, R., 2016. Improved bacterial 16S rRNA gene (V4 and V4-5) and fungal internal transcribed spacer marker gene primers for microbial community surveys. Msystems 1 (1), e00009–e00015.

Wang, Q., Garrity, G.M., Tiedje, J.M., Cole, J.R., 2007. Naive Bayesian classifier for rapid assignment of rRNA sequences into the new bacterial taxonomy. Appl. Environ. Microbiol. 73 (16), 5261–5267.

Wang, W., Ndungu, A.W., Li, Z., Wang, J., 2017. Microplastics pollution in inland freshwaters of China: a case study in urban surface waters of Wuhan, China. Sci. Total Environ. 575, 1369–1374.

Wang, Z., An, C., Chen, X., Lee, K., Zhang, B., Feng, Q., 2021. Disposable masks release microplastics to the aqueous environment with exacerbation by natural weathering. J. Hazard. Mater. 417, 126036.

Yoshida, S., Hiraga, K., Takehana, T., Taniguchi, I., Yamaji, H., Maeda, Y., Toyohara, K., Miyamoto, K., Kimura, Y., Oda, K., 2016. A bacterium that degrades and assimilates poly(ethylene terephthalate). Science 351 (6278), 1196–1199.

Zbyszewski, M., Corcoran, P.L., Hockin, A., 2014. Comparison of the distribution and degradation of plastic debris along shorelines of the Great Lakes, North America. J. Great Lakes Res 40 (2), 288–299.

Zettler, E.R., Mincer, T.J., Amaral-Zettler, L.A., 2013. Life in the "plastisphere": microbial communities on plastic marine debris. Environ. Sci. Technol. 47 (13), 7137–7146.